High-Temperature Polariton Lasing in a Strongly Coupled ZnO Microcavity

2012 Appl. Phys. Express 5 082801

(http://iopscience.iop.org/1882-0786/5/8/082801)

Applied Physics Express **5** (2012) 082801
http://dx.doi.org/**10.1143/APEX.5.082801**

High-Temperature Polariton Lasing in a Strongly Coupled ZnO Microcavity

Ying-Yu Lai, Yu-Pin Lan, and Tien-Chang Lu*

Department of Photonics, National Chiao Tung University, Hsinchu 300, Taiwan

Received June 16, 2012; accepted July 12, 2012; published online August 3, 2012

We report on the observation of polariton lasing in a negative detuned ZnO hybrid microcavity at room temperature (300 K) with threshold of 12.38 μJ/cm^2 and at high temperature (353 K) with a higher threshold of 53.05 μJ/cm^2 due to a stronger thermal escape process and a shallower polariton trap. The decoherence mechanism of the polariton laser due to the polariton self-interaction was investigated by power-dependent photoluminescence and Michelson interference measurements. The spatial coherence length $r_c \sim 0.26\,\mu$m of the polariton laser was obtained from Young's double slits. © 2012 The Japan Society of Applied Physics

Exciton-polaritons are bosonic quasi-particles, which can be generated from excitonic active layers embedded in semiconductor microcavities (MCs).[1] The bosonic nature allows exciton–polaritons to condense at the coherent ground state. The coherent light emission from a condensed polariton ground state, the so-called polariton laser, is driven by the stimulated scattering and needs no electronic population inversion condition as a conventional laser. Since the polaritons behave as weakly interacted bosons, the decoherence (or linewidth broadening) mechanisms of the polaritons in the condensate would occur due to the polariton self-interaction and number fluctuation.[2,3] Previously, polariton lasers have been demonstrated in GaAs,[4] CdTe,[5] and GaN MCs[6] from cryogenic temperature to room temperature (RT). Among wide-bandgap materials, the exciton binding energy of GaN is just comparable to the thermal energy at 300 K. In view of this, another wide-bandgap material, ZnO, is attractive for realizing a reliable RT polariton laser due to its large oscillator strength and exciton binding energy (~60 meV in the bulk ZnO).[7–9] The operation temperature of the exciton–polariton in a strongly coupled ZnO MC was observed up to 410 K.[10] To date, ZnO polariton lasers have been observed from 120 K with a small negative detuning ($\delta = -18$ meV)[11] to 300 K with a large negative detuning ($\delta = -119$ meV)[12] in planar ZnO bulk MCs and also in a single ZnO nanowire MC structure at RT.[13] However, the lasing characteristics such as temporal and spatial coherence are still absent. In this study, we employed the RT ZnO polariton lasing in a large negative detuned ZnO MC. The characteristics of polariton lasing such as polariton–polariton-induced linewidth broadening and decoherence mechanism were investigated by photoluminescence and Michelson interference measurements, respectively. The spatial coherence properties of localized polariton lasing were also determined by Young's double-slit measurement. Finally, we demonstrated the polariton lasing at temperatures up to 353 K.

The fabrication process of ZnO MC has been described elsewhere.[8] The scanning electron microscopy (SEM) image of the ZnO MC is shown in Fig. 1(a). The 30-pair AlN/AlGaN DBR was grown on a thick GaN buffer layer on a *c*-plane sapphire substrate. We employed 6-short-period GaN/AlN superlattice (SL) layers in every 3 to 5 AlN/AlGaN DBR pairs during the growth to suppress the tensile strain in the DBRs and achieve high reflectivity epitaxial DBRs with a wide stop-band width. The corresponding cross-sectional transmission electron microscopy (TEM) image of the SL layers is shown in Fig. 1(b). The $3/2\lambda$-thick ZnO active layer was grown on the AlN/AlGaN DBR using a pulsed KrF excimer laser ($\lambda = 248$ nm) deposition system at a working pressure of $\sim 9.8 \times 10^{-8}$ Torr without the oxygen gas flow. Finally, the 9-period SiO_2/HfO_2 dielectric DBR was deposited by dual electron-beam gun evaporation to complete the MC structure. The thickness nonuniformity in the ZnO cavity and nitride-based DBR provides different exciton-photon detunings.

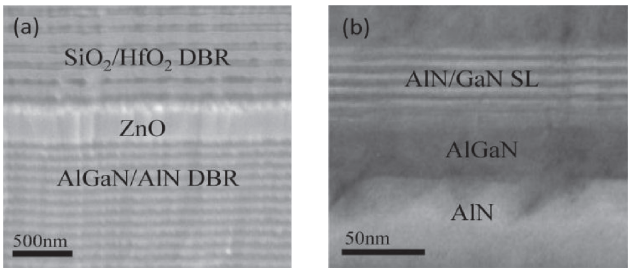

Fig. 1. (a) SEM image of the ZnO MC structure. (b) High magnification cross-sectional TEM image of one set of AlN/GaN SL insertion layers.

The angle-resolved photoluminescence (ARPL) measurement was carried out with a 355 nm Nd:YVO_4 pulse laser at a 1 kHz repetition rate and a pulse duration of 0.5 ns, which could be regarded as a quasi-CW excitation for polariton operation. The pumping laser spot size on the sample surface was about 60 μm in diameter at 60° incident angle. The polariton emission peaks extracted from ARPL spectra showed a Rabi splitting of ~100 meV at low excitation density [Fig. 2(a)]. Figure 2(b) shows that a nonlinear emission intensity occurs as the excitation density exceeds the threshold ($P_{th,R} \sim 12.38\,\mu$J/cm^2 per pulse). A slight emission energy blue shift of ~6 meV induced by the polariton–polariton interaction occurred between the polariton lasing mode and uncondensed LPB mode, as shown in Figs. 2(a) and 2(b). The value of the blue shift was smaller than the Rabi splitting and the separation between the lower polariton branch (LPB) and cavity mode (16 meV), confirming that the MC system was still operated in the strong coupling regime at $P_{th,R}$. Figure 2(c) shows an abrupt narrowing of the linewidth around the threshold, which could be interpreted as the spontaneous build-up of coherence phase in the condensate. Then, the linewidth of the polariton laser broadened with the excitation density after the threshold. In comparison, the single-mode photon laser, i.e., a noninteracting system, exhibited an extremely narrow linewidth

*E-mail address: timtclu@mail.nctu.edu.tw

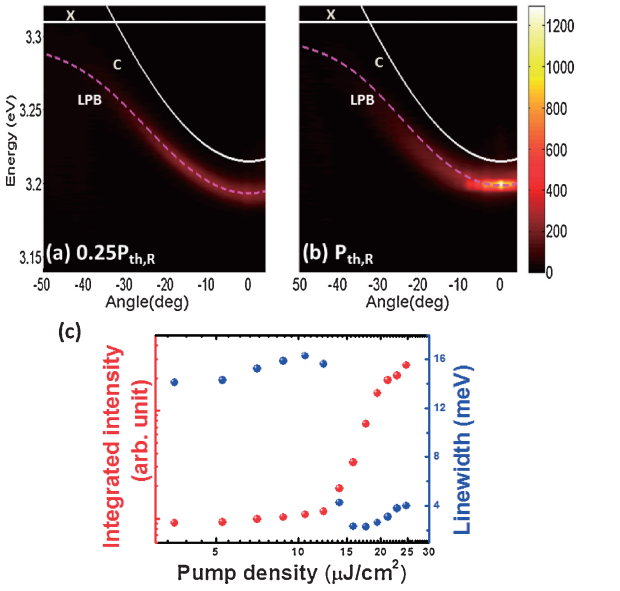

Fig. 2. Color maps of RT angle-resolved polariton emission at (a) $0.25P_{th,R}$ and (b) $P_{th,R}$, where X is the exciton mode, C is the photon mode or cavity mode, and LPB is the lower polariton branch. (c) Integrated intensity and linewidth of polariton emission versus pump intensity at RT.

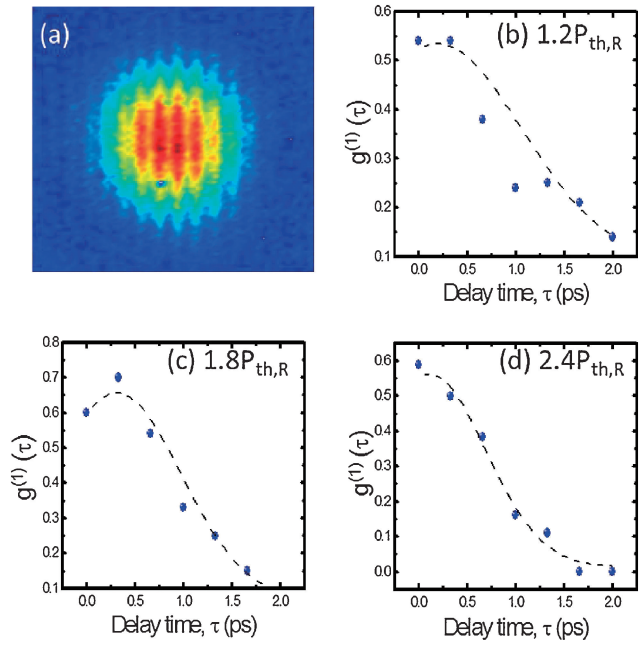

Fig. 3. (a) Interference pattern of polariton lasing. First-order degree of coherence $g^{(1)}(\tau)$ at (b) $1.2P_{th,R}$, (c) $1.8P_{th,R}$, and (d) $2.4P_{th,R}$.

that was inversely proportional to the output power.[14] In contrast, the excitonic nature enabled polaritons to interact with each other in the massive occupied ground state, which broadened the linewidth as the population of the ground state polariton increased.[2] In addition, the number fluctuation of interacting ground state polaritons arising from the intensity noise of the pump laser would lead to additional energy fluctuation to broaden the lasing linewidth.[3]

In order to study the linewidth broadening effect, we set up a normal Michelson interferometer to investigate the temporal decay properties of the polariton laser. The polariton laser emission passed into a Michelson interferometer, and the interference fringes were recorded using a charge-coupled device (CCD) [Fig. 3(a)]. The delay time could be adjusted by tuning the optical length difference in two arms of the Michelson interferometer. Figures 3(b) to 3(d) display the first-order temporal coherence $[g^{(1)}(\tau)]$ of the polariton laser at different pumping densities versus delay time. At $1.2P_{th,R}$, $g^{(1)}(\tau)$ had a Gaussian distribution with a coherence time $\tau_c \sim 1.22$ ps, fitted from $\exp(-\tau^2/\tau_c^2)$. From the measured coherence time τ_c, the corresponding linewidth ($\Delta\nu = 1/\tau_c$) of the polariton laser was about 3.4 meV. Once the pump intensity increased from 1.2 to $2.4P_{th,R}$, the coherence time τ_c decreased from 1.22 to 0.82 ps, and the calculated linewidth broadened from 3.4 to 5 meV. The decrease of coherence time of the polariton laser shows the consistent tendency with the linewidth broadening of the ARPL spectra, revealing evidence of the severe polariton–polariton interaction and number fluctuation as the population of the condensed polariton increased.[3] The temporal coherence property of uncondensed polaritons was hardly observed using the interferometer due to the much shorter coherence time (wider linewidth) and poor degree of coherence (random phase of uncondensed polariton emission).

Not only the temporal coherence, but the spontaneous build-up of spatial coherence is also a signature of the

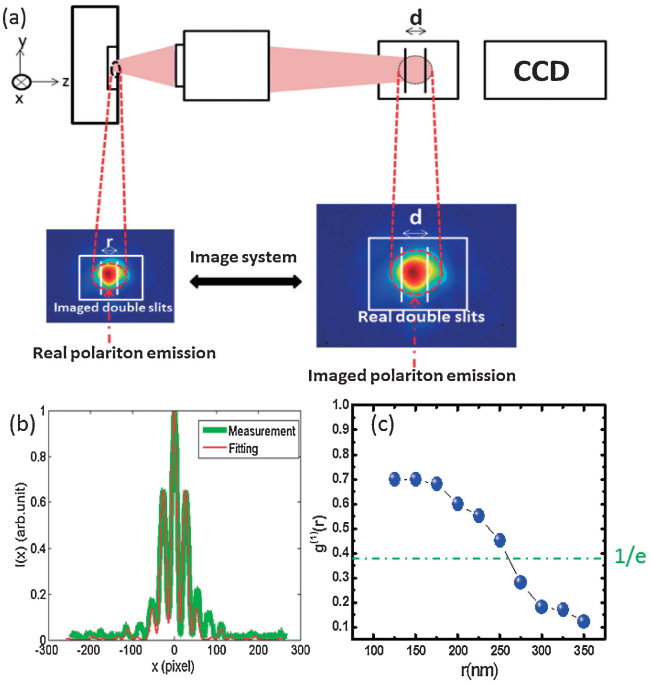

Fig. 4. (a) Sketch of the double-slit experiment setup. (b) Interference intensity distribution on CCD. (c) Degree of spatial distribution $g^{(1)}(r)$ versus imaged slit separation r.

polariton laser. We employed a common Young's double slit to observe the spatial coherence of the polariton laser at $1.1P_{th,R}$ as shown in Fig. 4(a). The polariton emission pattern was imaged onto a series of double slits with different slit separations d. The resulting interference patterns were recorded using the CCD. Figure 4(b) shows the intensity distribution of the recorded interference pattern at the CCD for $d = 150\,\mu$m, and the corresponding effective slit width and slit separation r seen by the polariton emission

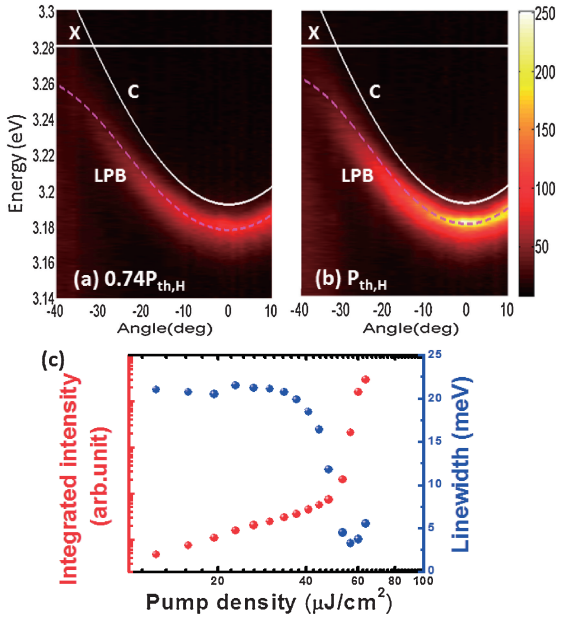

Fig. 5. Color maps of HT angle-resolved polariton emission at (a) $0.74P_{th,H}$ and (b) $P_{th,H}$. (c) Integrated intensity and linewidth of polariton emission versus pump intensity at HT.

on the sample surface were estimated to be 0.05 and 0.15 μm, respectively. The first-order spatial coherence $g^{(1)}(r) \sim 0.7$ of the polariton laser was fitted from the normal double-slit interference equation. Then, the spatial coherence of the polariton laser was systematically recorded and analyzed from a set of double slits with different slit separations d, and transferred to the effective slit separation r. Figure 4(c) shows $g^{(1)}(r)$ as a function of the slit separation at $1.1P_{th}$. The spatial coherence of the polariton laser decreased with increasing r. The effective separation of slits at $g^{(1)}(r) = 1/e$ is defined as the spatial coherence length r_c of the polariton laser. From Fig. 4(c), the spatial coherence length of the polariton laser r_c is about 0.26 μm which is much smaller than that of the GaAs system at cryogenic temperature[15,16] and comparable to those of other localized polariton lasing in ZnO MC.[11] The relatively small coherence length could be attributed to the larger in-plane spatial disorder of the ZnO layer or the RT operation since the de Broglie wavelength is inversely proportional to the square root of temperature.

We further explored the operation temperature of the polariton laser from 300 up to 353 K. At 353 K, the photon-exciton detuning of the ZnO microcavity decreased from −94 to −88 meV, and the corresponding Rabi splitting was about 86 meV. Figures 5(a) and 5(b) show the angle-resolved dispersion curves of polariton emission at 353 K with $0.74P_{th,H}$ and $P_{th,H}$, respectively. The power-dependent emission intensity and linewidth of the polariton are summarized in Fig. 5(c). The threshold pumping density $P_{th,H}$ was about 53.05 μJ/cm^2 (~106.1 kW/cm^2), which was still lower than that of the previously reported conventional photon lasing in a ZnO-based vertical cavity surface emitting laser structure at room temperature,[17] demonstrating the practical potential of polariton lasers. The higher threshold of the high-temperature polariton lasing than that of the RT case could be the result of a relatively shallow polariton trap and stronger thermal escape process caused by the higher temperature. The broadening of the polariton linewidth above the threshold could be due to the polariton number fluctuations and self-interactions of the ground-state polaritons similar to the RT case reported in the previous subsection.

We have shown the characteristics of RT polariton lasing in a hybrid ZnO MC and observed the polariton lasing behavior even at 353 K with a low threshold of 53.05 μJ/cm^2. It is the highest operation temperature of polariton lasing to our best knowledge. Spectral narrowing and spontaneous coherence build-up were clearly observed at the threshold. Above the threshold, the linewidth broadening and decrease of $g^{(1)}(\tau)$ induced by the polariton–polariton interaction and number fluctuation were presented as the increase of the ground-state polariton population. In addition, a Young's double-slit measurement showed the spatial coherence $g^{(1)}(r)$ of polariton lasing to be about 0.26 μm. These results demonstrate a milestone for realizing reliable and high-temperature-operated semiconductor exciton–polariton coherent light sources.

Acknowledgments The authors would like to gratefully acknowledge Professor H. Deng of Michigan University for her helpful suggestion and Professor S. C. Wang, Professor W. F. Hsieh, and Professor H. C. Kuo of National Chiao Tung University for technical support. This work was supported in part by the MOE ATU program and in part by the National Science Council of the Republic of China (ROC) in Taiwan under Contract NSC 100-2628-E-009-013-MY3.

1) C. Weisbuch, M. Nishioka, A. Ishikawa, and Y. Arakawa: Phys. Rev. Lett. **69** (1992) 3314.
2) D. Porras and C. Tejedor: Phys. Rev. B **67** (2003) 161310(R).
3) A. P. D. Love, D. N. Krizhanovskii, D. M. Whittaker, R. Bouchekioua, D. Sanvitto, S. Al Rizeiqi, R. Bradley, M. S. Skolnick, P. R. Eastham, R. André, and L. S. Dang: Phys. Rev. Lett. **101** (2008) 067404.
4) H. Deng, G. Weihs, D. Snoke, J. Bloch, and Y. Yamamoto: Proc. Natl. Acad. Sci. U.S.A. **100** (2003) 15318.
5) J. Kasprzak, M. Richard, S. Kundermann, A. Baas, P. Jeambrun, J. M. J. Keeling, F. M. Marchetti, M. H. Szymańska, R. André, J. L. Staehli, V. Savona, P. B. Littlewood, B. Deveaud, and L. S. Dang: Nature **443** (2006) 409.
6) S. Christopoulos, G. Baldassarri Höger von Högersthal, A. J. D. Grundy, P. G. Lagoudakis, A. V. Kavokin, J. J. Baumberg, G. Christmann, R. Butté, E. Feltin, J.-F. Carlin, and N. Grandjean: Phys. Rev. Lett. **98** (2007) 126405.
7) J. R. Chen, T. C. Lu, Y. C. Wu, S. C. Lin, W. R. Liu, W. F. Hsieh, C. C. Kuo, and C. C. Lee: Appl. Phys. Lett. **94** (2009) 061103.
8) J. R. Chen, T. C. Lu, Y. C. Wu, S. C. Lin, W. F. Hsieh, S. C. Wang, and H. Deng: Opt. Express **19** (2011) 4101.
9) M. Zamfirescu, A. Kavokin, B. Gil, G. Malpuech, and M. Kaliteevski: Phys. Rev. B **65** (2002) 161205(R).
10) C. Sturm, H. Hilmer, R. Schmidt-Grund, and M. Grundmann: New J. Phys. **11** (2009) 073044.
11) T. Guillet, M. Mexis, J. Levrat, G. Rossbach, C. Brimont, T. Bretagnon, B. Gil, R. Butté, N. Grandjean, L. Orosz, F. Réveret, J. Leymarie, J. Zúñiga-Pérez, M. Leroux, F. Semond, and S. Bouchoule: Appl. Phys. Lett. **99** (2011) 161104.
12) T. C. Lu, Y. Y. Lai, Y. P. Lan, S. W. Huang, J. R. Chen, Y. C. Wu, W. F. Hsieh, and H. Deng: Opt. Express **20** (2012) 5530.
13) A. Das, J. Heo, A. Bayraktaroglu, W. Guo, T. K. Ng, J. Phillips, B. S. Ooi, and P. Bhattacharya: Opt. Express **20** (2012) 11830.
14) C. H. Henry: IEEE J. Quantum Electron. **18** (1982) 259.
15) H. Deng, G. S. Solomon, R. Hey, K. H. Ploog, and Y. Yamamoto: Phys. Rev. Lett. **99** (2007) 126403.
16) C. W. Lai, N. Y. Kim, S. Utsunomiya, G. Roumpos, H. Deng, M. D. Fraser, T. Byrnes, P. Recher, N. Kumada, T. Fujisawa, and Y. Yamamoto: Nature **450** (2007) 529.
17) S. Kalusniak, S. Sadofev, S. Halm, and F. Henneberger: Appl. Phys. Lett. **98** (2011) 011101.